Single Conformation Spectroscopy of a Flexible Bichromophore: 3-(4-Hydroxyphenyl)-*N*-benzylpropionamide

Esteban E. Baquero,[†,‡] William H. James III,[†] Tae Hoon Choi,[§] Kenneth D. Jordan,*[,§] and Timothy S. Zwier*[,†]

Department of Chemistry, Purdue University, 560 Oval Drive, West Lafayette, Indiana 47907-2084, and Department of Chemistry, Chevron Science Center, University of Pittsburgh, 219 Parkman Avenue, Pittsburgh, Pennsylvania 15260

Received: July 30, 2008; Revised Manuscript Received: September 8, 2008

Resonant two-photon ionization (R2PI), UV hole-burning (UVHB), and resonant ion-dip infrared (RIDIR) spectroscopy have been used to study the single-conformation infrared and ultraviolet spectroscopy of 3-(4-hydroxyphenyl)-*N*-benzylpropionamide (HNBPA, $HOC_6H_5CH_2CH_2(C{=}O)NHCH_2C_6H_5$) cooled in a supersonic expansion. UVHB determines the presence of three conformers, two of which dominate the spectrum. RIDIR spectra in the OH stretch (3600−3700 cm^{-1}), amide NH stretch (3450−3500 cm^{-1}), and C=O stretch (1700−1750 cm^{-1}) regions reveal the presence of small shifts in these fundamentals that are characteristic of the folding of the flexible chain and the ring−ring and ring−chain interactions. On the basis of a comparison of the experimental frequency shifts with calculations, the two major experimentally observed conformers are assigned to two folded structures in which the two aromatic rings are (nominally) face-to-face and perpendicular to one another. The perpendicular structure has a transition assignable to the S_0-S_2 origin, while the face-to-face structure does not, consistent with a faster nonradiative process in the latter case. The calculated structures and vibrational frequencies are quite sensitive to the level of theory due to the flexibility of the interconnecting chain and the importance of dispersive interactions between the two aromatic rings.

I. Introduction

Recently, much effort has been focused on establishing the intrinsic conformational preferences of prototypical molecules of biological relevance.[1−5] By use of conformation-specific spectroscopy one can determine the spectral signatures of specific conformers, thereby gaining information about the potential energy surface governing the molecule of interest. An alternative strategy is to use conformation-specific spectroscopy to study molecules that, while not of direct biological relevance, possess features of their potential energy surfaces that may be relevant in biological macromolecules. In that spirit, we have recently investigated *O*-(2-acetamidoethyl)-*N*-acetyltyramine (OANAT, see below),[6] a molecule which possesses two flexible side chains positioned at opposite ends of a single phenyl ring, and found that, under jet cooling, strongly energetically disfavored conformers retain significant population due to entropy effects.

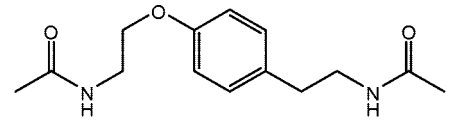

O-(2-acetamidoethyl)-N-acetyltyramine
(OANAT)

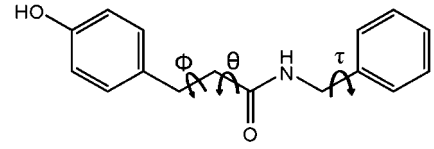

3-(4-Hydroxyphenyl)-N-Benzyl-Propionamide
(HNBPA)

In the present study, we examine the single-chain bichromophore, 3-(4-hydroxyphenyl)-*N*-benzylpropionamide (HNBPA). Our motivation in doing so is two-fold. First, HNBPA provides an opportunity to probe the delicate balance of steric constraints and dispersive forces involving the two aromatic rings and the chain that connects them. Accurate calculations of relative energies and vibrational spectra of the conformers of HNBPA is a challenge to modern electronic structure methods. Standard density functional theoretical (DFT) methods such as Becke3LYP[7−9] systematically underestimate dispersive interactions and, thus, do not properly describe folded structures.[10,11] On the other hand, the MP2 method,[12] which includes dispersion interactions, often overstabilizes folded structures.[6,11] This problem is further compounded by basis set superposition error (BSSE)[13] unless very large basis sets are employed. These issues have been extensively studied for the benzene dimer,[14−22] where the challenge is obtaining an accurate estimate of the relative energies of face-to-face and perpendicular structures. The presence of the bridging chain in HNBPA introduces new challenges beyond those present for the benzene dimer. In our theoretical study of HNBPA, we make use of the DFT B3LYP and MP2 electronic structure methods, and compose the results with DFT calculations employing the (M05-2X)[15,23,24] functional of Truhlar and co-workers, which has been designed to account for long-range dispersion interactions within a DFT framework.

Second, ultraviolet spectroscopy is used to probe conformation-specific electronic coupling between the two aromatic rings.

* Authors to whom correspondence should be addressed. E-mail: zwier@purdue.edu and jordan@a.psc.edu.
† Purdue University.
‡ Present address: Process Analytical, The Dow Chemical Company, 2301 N. Brazosport Blvd. B-1463, Freeport, Texas 77541.
§ University of Pittsburgh.

10.1021/jp806787p CCC: $40.75
Published on Web 10/14/2008

There is a rich tradition of ultraviolet spectroscopic studies of bichromophoric systems under jet-cooled conditions.[25−32] The electronic coupling between chromophores depends on the distance,[25−27] relative orientation,[26−31] and symmetry[32] of the chromophores, and manifests itself through exciton interactions. By design, most of these studies have focused on molecules with the chromophores connected by rigid[28] or semirigid frames,[29−32] which minimizes the conformational flexibility. There are fewer studies of molecules in which the chain connecting the conformers is intentionally flexible, requiring the application of conformer-specific methods to identify the conformations present prior to studying electronic energy transfer. The ground-breaking work of Zehnacker et al. had as its goal the study of excimer formation,[26,27] while Chattaraj et al.[29] used a semirigid frame (cyclohexane) to connect the chromophores, thereby restricting the possible orientations to some degree.

In the present study, conformation specific spectroscopy of HNBPA is carried out to gain further insight into how structural changes in a flexible bichromophore affect electronic coupling. HNBPA contains two spectroscopically distinguishable UV chromophores, the phenol and phenyl rings, that are bridged by a 5-membered chain containing a single amide group, which permits the chromophores to sample a variety of distances and orientations, resulting in conformation-specific rates of electronic energy transfer, and splittings between the S_1 and S_2 states. As we shall see, the two dominant observed conformers of HNBPA display significant spectroscopic differences, enabling us to observe the S_2 state in one case but not the other.

II. Methods

A. Experimental Overview. The experimental apparatus and spectroscopy methods used in this investigation has been described in detail elsewhere,[6] and only a brief description will be given here. The HNBPA sample obtained from Sigma-Aldrich had 96% purity and was used without any further purification. The solid sample was introduced into the gas phase by heating it to approximately 180−190 °C in a sample holder located directly behind the pulsed valve. A glass insert was placed inside the sample holder to minimize decomposition. The sample was expanded into the vacuum region via a pulsed valve (Parker General Valve, Series 9, 400 μm orifice, 20 Hz), using a 70%/30% neon/helium gas mixture as a carrier gas with a backing pressure of 1.7 bar. The collisionally cooled molecules were interrogated in the ionization region of a time-of-flight mass spectrometer (TOFMS) approximately 10 cm from the nozzle. The ionization and source regions are separated by a conical skimmer (Beam Dynamics, Inc., 55° conical angle, 2 mm diameter). Flow rates in the 0.15−0.30 bar·cm^3/s range were used to avoid skimmer interference.

Electronic spectra were recorded by employing one-color resonant two-photon ionization (R2PI). Conformation-specific electronic spectra were obtained by using UV−UV hole-burning (UVHB) spectroscopy, while conformation-specific IR spectra were obtained by using resonant ion dip infrared (RIDIR) spectroscopy.[6]

B. Calculations. To assist in the assignment of the observed conformers, electronic structure calculations were used to optimize the geometries and to obtain predictions for the relative energies of the different conformers of HNBPA. In addition, harmonic vibrational frequencies and IR intensities were calculated for comparison with experiment.

An initial search of the potential energy surface for HNBPA was performed by using the Amber[33] and MMFF[34] force fields as implemented in the MACROMODEL suite of programs.[35] These minima were then used as starting structures for geometry optimizations, using the B3LYP[36] DFT method together with the 6-31+G(d)[37] basis set. The B3LYP structures, in turn, were used as starting structures for optimization, using the MO5-2X and MP2 methods with the 6-31+G(d) basis set, as well as using the RIMP2[38] method with larger aug-cc-pVDZ and aug-cc-pVTZ basis sets.[39−41] Finally, for three conformers calculations were also carried out by using the DF-SCS-LMP2 method together with the aug-cc-pVDZ basis set. The spin-component-scaled (SCS) algorithm[42] has been found to greatly improve the performance of the MP2 method for systems such as the benzene dimer[19] whereas the use of localized (L) orbitals, using the Saebø−Pulay procedure,[43] eliminates much of the BSSE. It is worth noting that the RI and DF methods are fundamentally the same, referring to the use of auxiliary basis sets to speed up the calculations. The B3LYP, MO5-2X, and MP2 calculations were carried out with the GAUSSIAN 03 suite of programs. The RIMP2 and DF-SCS-LMP2 calculations were performed with the Turbomole[44] and Molpro[45] programs, respectively.

We leave to the Discussion section a full comparison of the structures, relative energies, and harmonic vibrational frequencies produced by the various methods. For the purposes of making conformational assignments, we use the M05-2X[15,23,24] method as a computationally tractable option for giving geometries and harmonic frequencies that are expected to be close to those from large basis set CCSD(T) calculations, were they feasible for HNBPA.

III. Results and Analysis

A. Conformation-Specific Spectroscopy. The top trace in Figure 1 shows the R2PI spectrum of HNBPA in the origin region between 35 336 and 36 036 cm^{-1}. The spectrum is very congested and is dominated by two sets of bands. The UVHB spectrum with the hole-burn laser fixed on the transition at 35 517 cm^{-1} (marked with an asterisk) establishes that all the transitions in this region belong to a single conformer with an S_0-S_1 origin at 35 368 cm^{-1} (Figure 1A). The vibrational structure of this conformer is dominated by Franck−Condon progressions and combination bands involving two vibrations of frequency 28 and 45 cm^{-1}. Two other fundamentals at 111 and 164 cm^{-1} serve as starting points for other progressions involving the low-frequency modes.

The UVHB spectrum with hole-burn laser fixed on the transition at 35 759 cm^{-1} (Figure 1B) shows this band to be the S_0-S_1 origin of a second conformer with vibronic progressions built off the origin that encompass most of the remaining bands unaccounted for by conformer A. This conformer shows much shorter Franck−Condon progressions due to vibrations with 16, 18, and 31 cm^{-1} frequencies.

Comparison of the R2PI and UVHB spectra of HNBPA shown in Figure 1, reveals weak transitions in the R2PI spectrum that did not burn with either conformer A or B. These bands at 35 601 and 35 613 cm^{-1} are located between the vibronic transitions of the two major conformers. UVHB measurements on these bands (not shown) indicate that they too belong to a single conformer (C). The proximity of these bands to transitions from the higher population conformers prevented us from characterizing them with conformation-specific IR spectroscopy and from assigning the S_0-S_1 origin transition for conformer C. Therefore, in the remainder of this paper, we will concentrate on the two major conformers (A and B).

To learn more about the geometrical structures responsible for the two major conformers, resonant ion-dip infrared (RIDIR)

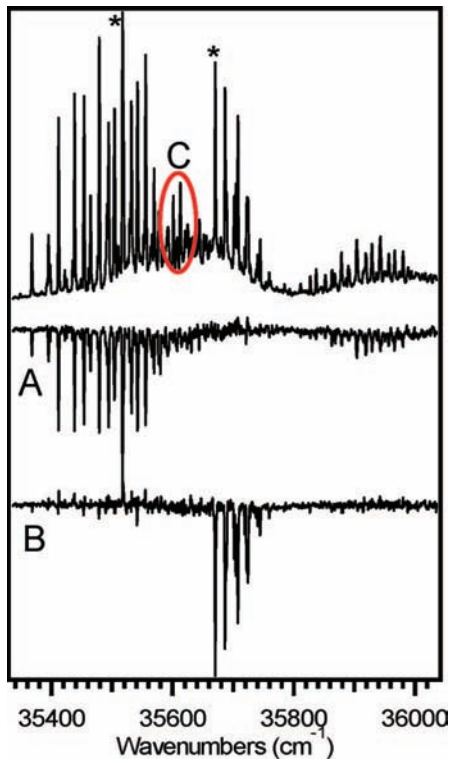

Figure 1. Top trace: The R2PI spectrum of HNBPA. Bottom two traces: The UV−UV hole-burning spectra of conformers A and B, respectively. Transitions due to a minor conformer, conformer C, are circled on the top trace. The asterisks denote the transitions used as the hole-burn transition in each case.

spectra were recorded in the amide NH stretch region (Figure 2a, 3450−3550 cm^{-1}). The NH stretch fundamental of conformer A occurs at 3467 cm^{-1}, which is red-shifted by 11 cm^{-1} from the corresponding transition in conformer B (3478 cm^{-1}). The OH stretch fundamental (Figure 2b) of conformer A occurs at 3644 cm^{-1}, which is 10 cm^{-1} lower in frequency than that for conformer B (3654 cm^{-1}). S_0-S_1 origins and infrared bands for the two major conformers are summarized in Table 1.

There are several previous conformation-specific studies of the infrared spectroscopy of amide-containing molecules cooled in supersonic expansions.[1−6,46−49] However, none of the previously studied systems has the same chemical environment for the amide NH as HNBPA in which the amide group is separated from the phenyl ring by a single carbon atom. As a result, we recorded R2PI and RIDIR spectra of *N*-benzylacetamide (shown below), an analogue of HNBPA without the $CH_2C_6H_5OH$ group. This allows us to establish the experimental value of the free NH stretch fundamental of a chemically identical amide group in the case that there is no interaction with a second aromatic ring.

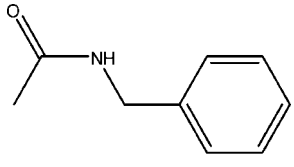

N-benzylacetamide

The R2PI spectrum of *N*-benzylacetamide (Figure 3) is dominated by a transition at 37 581 cm^{-1}, ascribed to the lowest energy conformation of the molecule, the structure (from RIMP2

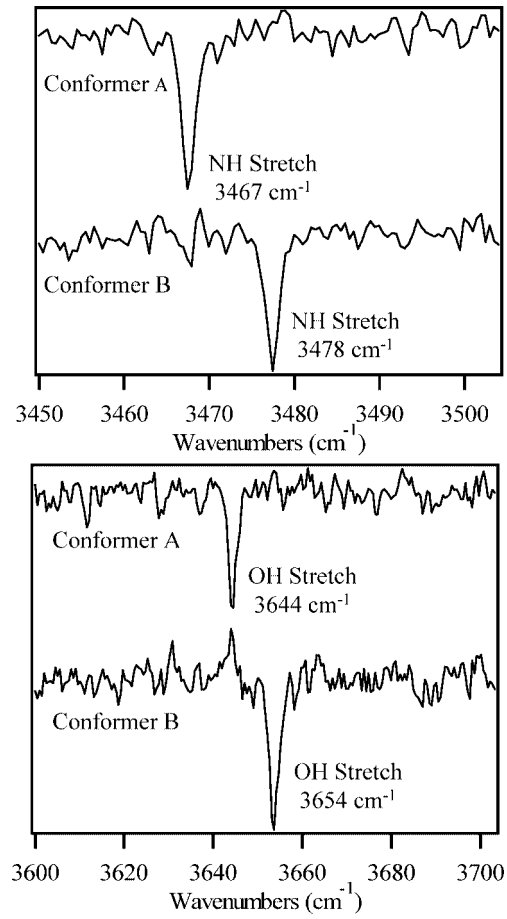

Figure 2. RIDIR spectra of conformers A and B of HNBPA. The top panel shows the amide NH stretch region (3450−3500 cm^{-1}), and the bottom panel shows the OH stretch region (3600−3654 cm^{-1}).

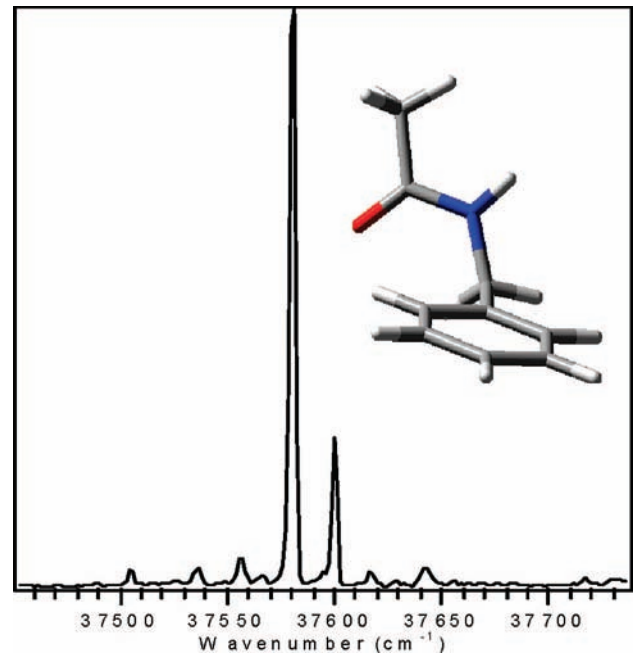

Figure 3. R2PI spectrum of *N*-benzylacetamide in the S_0-S_1 origin region.

calculations) of which is included as an inset in the figure. The geometry of the RIMP2 calculated structure of *N*-benzylacetamide was found to be nearly identical to that of the corresponding part of the chain (i.e., the phenyl ring through amide group)

TABLE 1: Experimentally determined $S_1 \leftarrow S_0$ Origins and IR Bands of the Two Major Conformers of HNBPA

conformer	$S_1 \leftarrow S_0$ origins (cm^{-1})	NH stretch (cm^{-1})	OH stretch (cm^{-1})
A	35368	3467	3644
B	35759	3478	3654

in the extended conformers of HNBPA. The RIDIR spectrum of *N*-benzylacetamide in the NH stretch region (not shown) consists of a single transition at 3483 cm^{-1}, which we take as the "zero" of our amide NH stretch frequency scale in the ensuing discussion. Relative to this "zero", conformers A and B of HNBPA have amide NH stretch fundamentals that are shifted by −18 and −8 cm^{-1}, respectively, from that of *N*-benzylacetamide.

The same comparisons can be made in the OH stretch region, this time with *p*-cresol as the reference (for which the free OH stretch fundamental appears at 3658 cm^{-1}).[50−53] The OH stretch fundamental of conformers A and B is thus shifted by −14 and −4 cm^{-1}, respectively, from that of *p*-cresol.

Figure 4 shows the RIDIR spectra of conformers A and B of HNBPA in the 1425−1795 cm^{-1} mid-infrared region. These spectra display several bands between 1530 and 1550 cm^{-1} that are attributed to the amide II (amide NH bend) vibrations and to in-plane CH bend modes of the aromatic rings. In the amide I region, the C═O stretch of conformer A appears at 1706 cm^{-1}, while the analogous band in conformer B has its maximum at 1712 cm^{-1}.

B. Calculated Minima and Comparison to Experiment. For each level of theory employed, eight distinct conformers were found. The structures obtained by using the MO5-2X method are shown in Figure 5, and their relative energies and the key structural parameters involving the dihedral angles (θ, ϕ, and τ, see Figure 5) of the chain, phenol, and phenyl rings are listed in Table 2. These structures can be arranged into conformational families based on the distance and the relative orientation between the chromophores. Four of the conformers, structures **V**−**VIII** in Figure 5, have the two aromatic rings far from one another ($R_{\pi-\pi}$ = 10−11 Å, the distance between the aromatic ring centers), and are referred to as extended. By contrast, the optimized structures **I**−**IV** shown in Figure 5 have the two aromatic rings close to one another ($R_{\pi-\pi}$ = 4−5 Å), and are referred to as "folded". The two aromatic rings in the folded and extended conformers can be found in either parallel ("facing") or perpendicular orientations. In addition, the conformers can differ in the orientation of the OH group on the phenol ring, referred to as "*cis*" or "*trans*" relative to the amide NH, leading to the eight conformers shown in Figure 5. The calculated energies of the *cis* and *trans* conformers of a given pair are close in energy to one another, except for the folded facing pair, which differ by just over 1 kcal/mol.

In the M05-2X calculations, the 4-folded conformers are 2−3.5 kcal/mol lower in energy than the four extended conformers. The calculated global minimum, fol-fac-TNH, is closely followed by the fol-per-TNH conformer, 0.30 kcal/mol higher in energy. The four extended conformers are calculated to lie within 0.1 kcal/mol of one another. Furthermore, the extended conformers have more low-frequency vibrations that can lead to stabilization due to zero-point contributions and entropic effects. As a result, at the expansion temperature (T = 190 °C) the extended conformers are predicted to be slightly lower in free energy than the folded conformers, leading us to expect both extended and folded conformers to have significant population in the pre-expansion region.

Table 3 compares the measured frequency shifts and corresponding predictions for the NH, OH, and C═O stretch vibrations at the DFT/M05-2X/6-31+G* level of theory. The calculated frequency shifts are reported relative to the same "zeros" used experimentally, namely, the OH stretch vibrational frequency for *p*-cresol and the NH stretch of *N*-benzylacetamide calculated at the same level of theory. Since the C═O stretch of *N*-benzylacetamide was not recorded, only the relative shift is relevant, so we take the lowest frequency C═O stretch as the "zero".

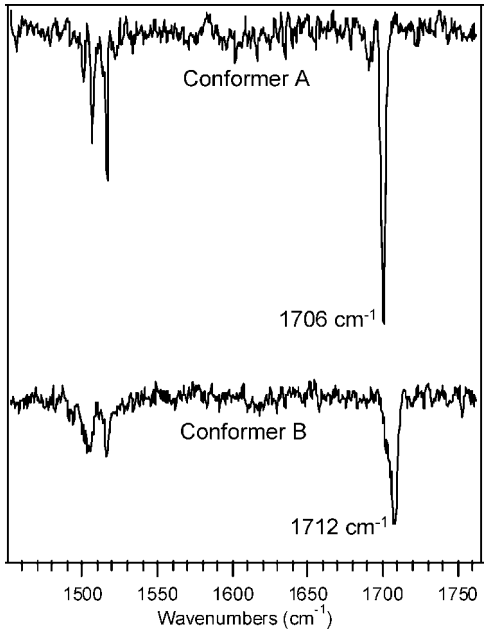

Figure 4. RIDIR spectra of HNBPA conformers A and B in the NH bend (~1500 cm^{-1}) and carbonyl stretch (~1700 cm^{-1}) regions.

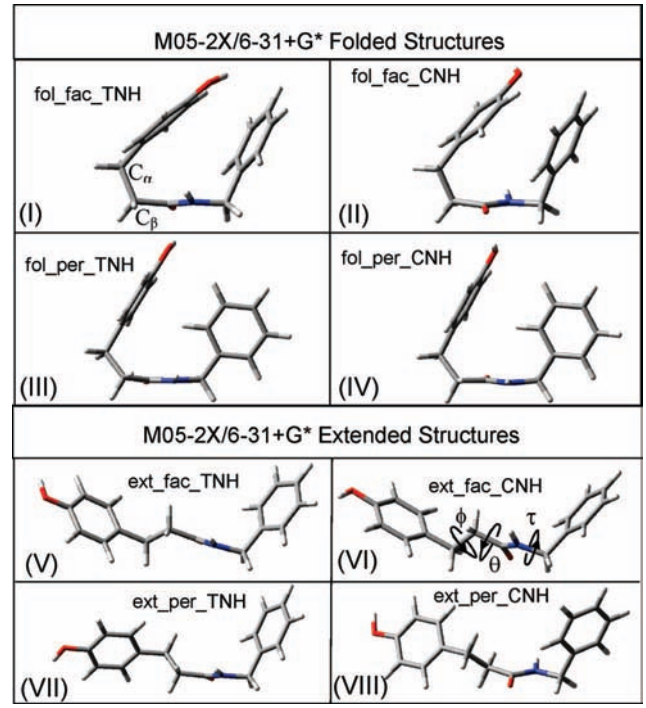

Figure 5. Optimized structures for the eight low-lying conformational minima of HNBPA calculated at the DFT M05-2X/6-31+G* level of theory. The $C_\alpha - C_\beta$ bond is shown in structure **I**. The dihedral angles used to describe the structures are shown in structure **VI**.

TABLE 2: Relative Energies and Structural Details for the Eight Minima of HNBPA at the DFT M05-2X/6-31+G* Level of Theory

structure	nomenclature	ΔE (kcal/mol)	ΔG at 190 °C (kcal/mol)	θ (deg)	ϕ (deg)	τ (deg)	$R_{\pi-\pi}$ (Å)	$R_{NH-\pi}$ (Å)	angle between ring planes (deg)
I	fol-fac-TNH	0.00	0.51	102.3	58.6	86.0	4.3	3.0	27.6
II	fol-fac-CNH	1.14	0.79	105.1	63.5	86.5	4.6	3.3	144.6
III	fol-per-TNH	0.30	1.08	127.1	59.5	39.6	5.1	3.9	99.0
IV	fol-per-CNH	0.65	0.82	129.9	61.3	43.5	5.1	3.9	88.0
V	ext-fac-TNH	3.39	0.26	139.6	175.8	66.7	11.3	5.3	110.2
VI	ext-fac-CNH	3.48	0.00	141.3	175.9	66.1	11.2	5.4	111.3
VII	ext-per-TNH	3.42	0.01	132.1	176.0	65.2	10.8	5.8	86.4
VIII	ext-per-CNH	3.48	0.38	139.2	176.9	114.5	11.0	5.3	97.4

TABLE 3: Experimental and Calculated (M05-2X) Frequency Shifts (in cm^{-1}) and Relative Vertical $S_1 \leftarrow S_0$ Separations (cm^{-1})[a]

		NH	OH	C=O	$S_1 \leftarrow S_0$
	Experimental				
	conformer A	−19	−14	−8	0
	conformer B	−8	−4	−2	391
	Calculated				
I	fol-fac-TNH	−28	−14	−8	0.0
II	fol-fac-CNH	−20	1	−8	172.9
III	fol-per-TNH	−12	−5	−3	381.6
IV	fol-per-CNH	−6	−4	−1	367.1
V	ext-fac-TNH	−10	2	−5	286.0
VI	ext-fac-CNH	−9	1	−5	273.4
VII	ext-per-TNH	−1	1	−7	295.0
VIII	ext-per-CNH	−1	2	−6	275.2

[a] The shifts in the NH, C=O, and OH stretch frequencies are given relative to the corresponding frequencies of *N*-benzylacetamide and *p*-cresol. The measured and calculated $S_1 \leftarrow S_0$ separations are reported relative to conformer A and structure **I**, respectively.

Comparison of the experimental and calculated frequency shifts in Table 3 supports an assignment of conformer A to the folded facing *trans*-NH structure **I**, and conformer B to the folded perpendicular *trans*-NH structure **III**. Specifically, we note that only structure **I** has the OH group in close enough proximity to the phenyl ring and with the correct orientation to produce a frequency shift as large as -14 cm^{-1}. Second, the pattern of frequency shifts associated with the NH, OH, and C=O stretch modes is faithfully reproduced by this pair of structures. Structure **III** (fol-perp-TNH) is calculated to have an NH stretch frequency shift about half that of structure **I**, a small but nonzero OH stretch shift, and a C=O stretch shifted to higher frequency by 5 cm^{-1}, in close agreement with the experimental trends. We note also that TD-DFT M05-2X/6-31+G* calculations predict the S_0-S_1 vertical excitation energy of **III** to be 381 cm^{-1} above that of **I**, while the experimental measurements place the origin of the S_1-S_0 transition of B 391 cm^{-1} above that of A. An alternative assignment of conformer B to **IV** cannot be entirely ruled out, since it shares the same overall trends in vibrational frequency shifts as **III**.

The UVHB spectra provide supporting evidence for these assignments. The UVHB spectrum of conformer A (Figure 1) shows long progressions involving 28 and 45 cm^{-1} low-frequency modes, indicating a large geometry change between S_0 and S_1. This is consistent with an assignment to a folded-facing conformer, with a geometry well situated for the two aromatic rings to be drawn together upon electronic excitation, leading to long progressions in low-frequency modes. By contrast, the S_0-S_1 origin transition in conformer B is the most intense vibronic band in the low-frequency region, with short Franck−Condon progressions in vibrations with 16, 18, and 31 cm^{-1} spacings. The folded perpendicular geometry would have a weaker interaction between the two rings, leading to a smaller geometry change. Admittedly, however, extended structures would also be expected to have weak Franck−Condon progressions.

IV. Discussion

A. Conformational Preferences of HNBPA. We have spectroscopically characterized two conformers of HNBPA, assigning conformer A to the folded facing structure **I** (Figure 5) calculated as the global minimum at the DFT M05-2X/6-31+G* level of theory. Conformer B has been tentatively assigned to the folded perpendicular structure **III**, which also happens to be the second most stable conformer at this level of theory. According to the M05-2X calculations, there are four folded structures within 1 kcal/mol and four extended structures about 3.5 kcal/mol higher in energy. We argued earlier that the populations in the pre-expansion gas mixture at $T = 190$ °C would be expected to be split about equally between folded and extended conformers. On the basis of our spectroscopic deductions, the downstream populations in the expansion in HNBPA are those predicted by DFT M05-2X calculations to be the two lowest energy folded conformers (and a minor amount of a third conformer that has not been spectroscopically characterized). On this basis, it is likely that the several higher energy extended structures that also have pre-expansion population are separated from these two lowest energy structures by the existence of low-energy barriers that facilitate funneling the population into the lowest energy wells during the collisional cooling in the expansion.

On the basis of similar reasoning, it is possible that the lowest energy pathways between the *cis*/*trans* pairs of conformers are not associated with the hindered rotation of the OH group (which in phenol derivatives is about 800 cm^{-1}) but instead involve internal rotation of the entire phenol ring relative to the frame of the amide-containing chain. Barriers of a few hundred cm^{-1} are a small fraction of the average total energy available to HNBPA at the pre-expansion temperature, suggesting that the higher energy of each *cis*−*trans* conformer pair would cool to its lower energy counterpart under expansion cooling. In seeking a more detailed understanding of the conformational preferences of HNBPA, a full disconnectivity diagram,[54] calculated by using accurate electronic structure methods, would be useful.

B. Contributions to the Observed Frequency Shifts. The assignments given above for the two major conformers of HNBPA were based on a comparison of the experimental frequency shifts for the NH, OH, and C=O stretch fundamentals with the values calculated for the eight conformers shown in Figure 5. The observed frequency shifts (2−18 cm^{-1}) are modest in size, but are nevertheless characteristic signatures. Here we look more closely at the sources of the frequency shifts.

Inspection of Table 3 shows that the two structures calculated to have the largest frequency shifts from the free amide NH value are the two folded-facing structures **I** and **II**. These structures both have θ dihedral angles close to 100°, which places the $C_\alpha-C_\beta$ bond (where α refers to the first alkyl carbon from the phenol ring, Figure 5) nearly perpendicular to the amide plane. As a consequence, the amide NH is brought into closer proximity to the phenol ring in **I** and **II** than in the other conformers of HNBPA, with $R_{NH-\pi} \approx 3$ Å (Table 2). There are two possible consequences of this: (1) in these orientations hyperconjugation with the $C_\alpha-C_\beta$ bond could be important, and (2) there could be a direct interaction of the amide group with the phenol ring. To assess the importance of hyperconjugation on the NH and C═O stretch vibrational frequencies, the frequencies were calculated for *N*-benzylpropionamide (NBPA) for a range of θ dihedral angles which varies the position of the terminal methyl group relative to the amide plane.

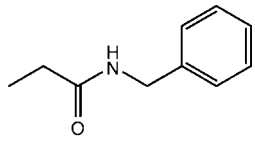

N-benzylpropionamide

The results of these calculations are depicted in Figure 6. As expected, the NH stretch frequency of NBPA shows a systematic dependence on the folding dihedral angle θ, decreasing by ~10 cm^{-1} as the dihedral angle is decreased from 140° to 100°, with the latter corresponding approximately to that in the folded facing conformers of HNBPA. This frequency shift is caused by hyperconjugation between the $C_\alpha-C_\beta$ bond and the C═O group. The C═O stretch frequency shows the inverse correlation, increasing in frequency as θ approaches 90°. The main structural difference between conformers **I** and **III** is the value of θ, and the shifts in both the NH and C═O stretch vibrations provide signatures of this angle.

The calculated frequency shifts of the NH stretch fundamental associated with the two folded-facing conformers of HNBPA (−28 cm^{-1} for **I** and −20 cm^{-1} for **II**) are approximately twice that in NBPA, indicating that interaction of the amide NH with the phenol ring also makes a significant contribution to the frequency shift. As noted above, structures **I** and **II** have the NH group pointed toward the phenol ring with $R_{NH-\pi} \approx 3$ Å. By comparison, the six other HNBPA conformers have NH stretch frequency shifts consistent with the absence of one or both of the hyperconjugation (θ) and NH−π interactions. For example, the folded perpendicular pair (**III** and **IV**) of conformers have θ dihedral angles near 130°, which essentially eliminates the shift due to hyperconjugation, but retains sufficiently small NH−phenol ring separations to cause ~10 cm^{-1} shifts in the frequencies of the NH stretch fundamentals.

The OH stretch frequency shift is a sensitive indicator of the close proximity of the phenyl ring to the phenol ring. All extended structures have calculated OH stretch frequencies shifted by no more than a couple of cm^{-1} from the value in *p*-cresol. Of the folded conformers, only in the *trans*-NH folded facing structure **I** is there a sizable interaction of the OH group with the phenyl π cloud, producing a small 15 cm^{-1} red shift in the OH stretch frequency. The folded perpendicular structures display small (5−6 cm^{-1}) red shifts of the amide HN stretch vibration, presumably due to an indirect interaction of the perpendicular phenyl ring with the phenol OH group.

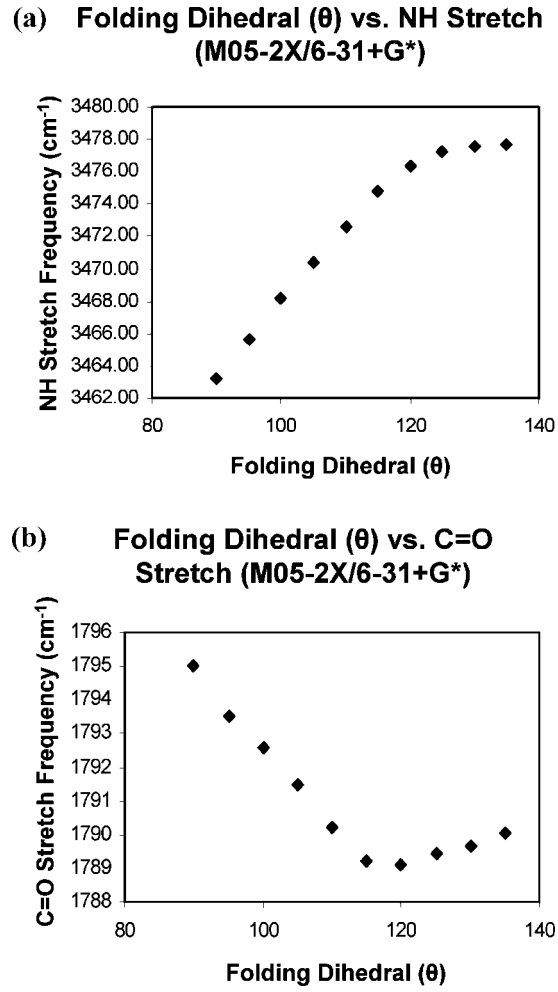

Figure 6. Graphical representation of the dependence of the calculated amide NH and CO stretch frequencies of HNBPA on the folding dihedral angle, θ, at the M05-2X/6-31+G* level of theory.

C. HNBPA as a Testing Ground for Theoretical Methods. From the outset, the contention has been that the combination of two aromatic chromophores linked by a flexible chain makes HNBPA a challenging and valuable test system for electronic methods for describing the geometries, relative energies, and spectroscopic signatures of large, flexible molecules. Our choice of the M05-2X/6-31+G* method was motivated by the recent work of Shields and van Mourik,[11] who suggested it as a reasonably accurate alternative to large basis set LMP2 or LCCSD(T0) calculations.

Indeed, we were drawn down this pathway in part by the DFT and MP2 results for the amide NH stretch frequency shifts of HNBPA. Table 4 reports the NH and OH stretch frequency shifts at the B3LYP/6-31+G*, MP2/6-31+G*, RIMP2/aug-cc-pVDZ, and M05-2X/6-31+G* levels of theory. It is obvious from the table that the B3LYP calculations fail to describe the subtle frequency shifts accompanying the structural changes in HNBPA, with the calculated frequency shifts being much smaller than experimentally observed. In contrast, the MP2 and RIMP2 calculations produce much larger frequency shifts than observed experimentally, with the larger errors in the RIMP2 calculations being due to the use of the larger basis set (Table 4). In keeping with the results on HNBPA, the θ-dependency of the frequency shifts in NBPA are underestimated with the B3LYP/6-31+G* calculations and overestimated in the MP2/6-31+G* calculations, with the values obtained from the DFT M05-2X calculations striking a balance between these two

TABLE 4: Calculated Frequency Shifts (cm^{-1}) at Different Levels of Theory[a]

	B3LYP/6-31+G* stretches (cm^{-1})		MP2/6-31+G* stretches (cm^{-1})		RIMP2/aug-cc-pVDZ stretches (cm^{-1})		M05-2X/6-31+G* stretches (cm^{-1})	
conformation	NH	OH	NH	OH	NH	OH	NH	OH
fol-fac-TNH	−1	0	−21	−19	−58	−34	−14	−8
fol-fac-CNH	N/A	N/A	−22	−9	−54	−10	1	−8
fol-per-TNH	−3	−4	−2	−9	−9	−11	−5	−3
fol-per-CNH	−3	0	−3	−8	−13	−7	−4	−1
ext-fac-TNH	−6	0	−2	−1	−9	0	2	−5
ext-fac-CNH	−6	0	−3	−1	−10	0	1	−5
ext-per-TNH	−3	0	−8	−1	−25	−1	1	−7
ext-per-CNH	−3	0	−8	−1	−25	0	2	−6

[a] The NH and OH shifts are reported relative to those of *N*-benzylacetamide and *p*-cresol, respectively.

TABLE 5: Relative Energies (kcal/mol) and Structural Details for the Conformers of HNBPA at DiffErent Levels of Theory

	B3LYP/6-31+G*			MP2/6-31+G*			RIMP2/aug-cc-pVDZ			RIMP2/aug-cc-pVTZ			M05-2X/6-31+G*		
conformation	ΔE	θ (deg)	$R_{\pi-\pi}$ (Å)	ΔE	θ (deg)	$R_{\pi-\pi}$ (Å)	ΔE	θ (deg)	$R_{\pi-\pi}$ (Å)	ΔE	θ (deg)	$R_{\pi-\pi}$ (Å)	ΔE	θ (deg)	$R_{\pi-\pi}$ (Å)
fol-fac-TNH	0.88	126.4	5.8	0.00	99.5	4.2	0.00	95.7	4.1	0.00	95.7	4.2	0.00	102.29	4.3
fol-fac-CNH	N/A	N/A	N/A	0.95	99.4	4.2	1.28	94.7	4.1	1.13	94.7	4.1	1.14	105.05	4.6
fol-per-TNH	0.00	133.7	6.7	2.09	125.8	4.9	2.07	126.7	4.7	1.95	127.0	4.8	0.30	127.05	5.1
fol-per-CNH	0.14	133.0	6.5	1.80	124.0	3.5	2.63	122.7	3.3	2.00	123.2	3.4	0.65	129.89	5.1
ext-fac-TNH	0.31	133.9	11.6	7.90	129.8	11.1	10.89	126.0	11.2	8.37	128.2	11.1	3.39	139.55	11.3
ext-fac-CNH	0.39	133.6	11.6	7.97	131.5	11.0	10.95	128.8	11.2	8.42	129.5	11.2	3.48	141.27	11.2
ext-per-TNH	0.31	133.0	11.2	7.72	108.7	9.6	10.40	100.5	9.3	8.16	109.1	9.8	3.42	132.10	10.8
ext-per-CNH	0.40	133.5	11.7	7.82	108.7	9.5	10.47	100.5	9.3	8.22	109.2	9.8	3.48	139.17	11.0

extremes. Quantitative comparisons can be drawn from the structural comparisons presented in Table 5, where the chain folding dihedral angle, θ, and ring−ring distance, $R_{\pi-\pi}$, calculated by using the various theoretical methods, are presented.

The trends in the optimized geometries are consistent with those noted above for the frequencies;[11] namely, with the MP2 and RIMP2 methods, the folded structures have much smaller ring−chain and ring−ring distances than the corresponding B3LYP results. The MO5-2X calculations give ring−chain and ring−ring distances intermediate between those from the B3LYP and MP2 calculations. This is also in keeping with previous computational results for the structures and binding energies of intermolecular complexes such as the benzene dimer,[17] phenol dimer,[16] and phenol−methanol.[18] These structural differences are shown pictorially in Figure 7, where the optimized structures of **I** and **III** at the B3LYP/6-31+G* and RIMP2/aug-cc-pVDZ levels of theory are overlaid. Interestingly, the geometry changes in going from the RIMP2/aug-cc-pVDZ to the RIMP2/aug-cc-pVTZ optimized structures are quite small. It seems likely, then, that the major deficiency of these calculations is the overestimation of dispersion interactions rather than the presence of BSSE.

Shields and van Mourik have argued that localized MP2 or localized CCSD(T0) calculations with the aug-cc-pVTZ basis set are sufficiently accurate for addressing the sorts of issues raised in the present study. However, while the use of localized orbitals, with the Saebø and Pulay scheme for generalizing the excitations,[43] does reduce the BSSE, it does not solve the problem of the tendency of the MP2 method to overestimate correlation effects between parallel (or near parallel) aromatic ring systems. Also, we have found that both LMP2 and LCCSD(T0) calculations, as normally carried out, localize the π orbitals of the aromatic rings in one of their resonance structures, which can introduce errors in the geometries and relative energies. It is for these reasons that we chose to use calculations with the M05-2X DFT function for our analysis. As noted above, the geometries of HNBPA optimized with the MO5-2X and BLYP/DCACP methods are intermediate between those obtained by using the B3LYP and MP2 (or RIMP2) methods. Furthermore, the trends in the vibrational frequency shifts calculated with the MO5-2X approach are in good agreement with experiment, for the proposed assignment.

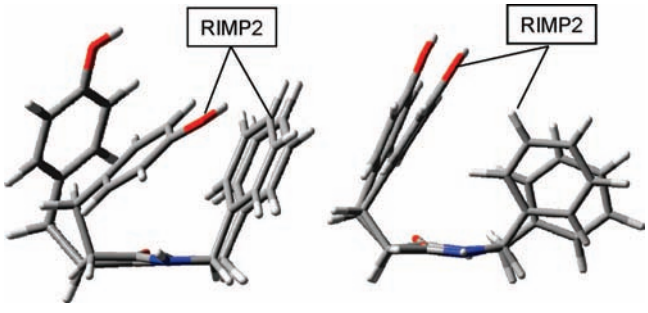

Figure 7. Overlaid folded facing (**I**) and perpendicular (**III**) structures optimized at the B3LYP/6-31+G* and RIMP2/aug-cc-pVDZ levels of theory.

Figure 8 reports the relative energies of the eight conformers as calculated with different electronic structure methods. As expected on the basis of the earlier discussion, the MP2 calculations strongly favor the folded structures, with the energy difference between the folded and extended structures being about 8 kcal/mol at the RIMP2/aug-cc-pVTZ level, while with the B3LYP method the folded and extended structures are quite close in energy. In contrast, the DFT/M05-2X calculations predict the energetic difference between folded and extended conformers to be ∼3.5 kcal/mol, with the folded structures being favored.

Figure 9 also includes relative energies calculated with the DF-SCS-LMP2/aug-cc-pVDZ level of theory. Interestingly, the relative energies obtained from this approach are quite close to the MO5-2X results. We note also that these two approaches give similar geometries. In the case of conformers **I**, **III**, and **VII** and for the two reference compounds we also calculated vibrations using the DF-SCS-LMP2 method, obtaining frequency shifts for **I**, **III**, and **VII** close to the MO5-2X results, further supporting the use of the MO5-2X method for making the assignments.

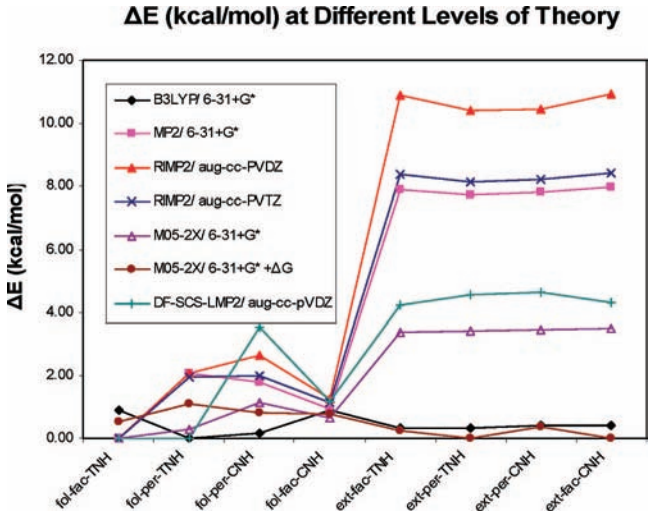

Figure 8. Relative energies of eight low-energy conformers of HNBPA calculated by using the indicated theoretical methods, computed at the optimized geometries for each method.

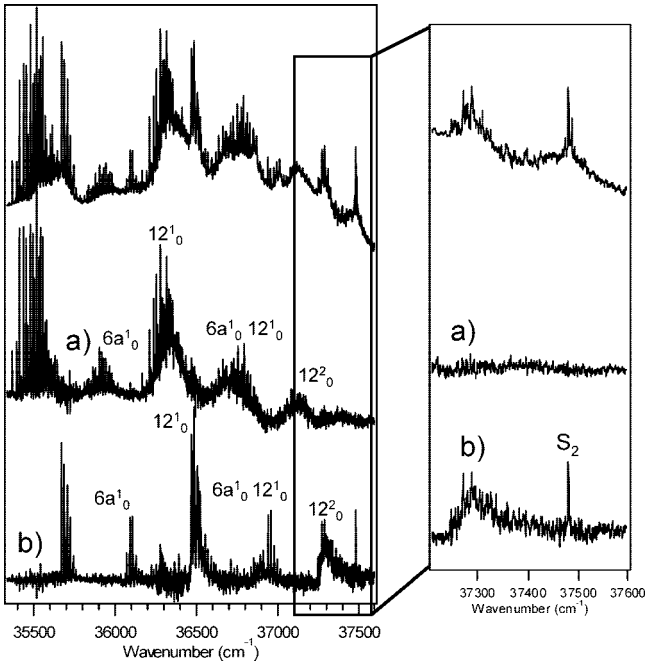

Figure 9. Top trace: Overview R2PI spectrum of HNBPA. (a and b) The overview UV hole-burning spectra of conformers A and B, respectively. (b) The 400 cm^{-1} spacing between vibronic clumps built off phenol ring breathing modes. This spacing is cut in half between the last vibronic clump and the S_2 state.

D. Conformation-Dependent Electronic Coupling. One of the motivations for this study was the possibility of observing conformer-specific electronic coupling in the excited states. According to Förster theory and its theoretical extensions,[55] the efficiency of electronic energy transfer between two electronic chromophores depends on the energy gap and the relative distance and orientation of the chromophores.[25−32] Figure 9 displays overview R2PI and UVHB spectra of conformers A and B of HNBPA taken over a region stretching to ∼2300 cm^{-1} above the S_0-S_1 origin of conformer A. Assignments for the main vibronic bands built off the S_1 origin can be made by comparison with phenol and *p*-cresol, whose UV spectroscopy has been studied in some detail. The vibrational numbering scheme is that introduced by Wilson to describe the benzene-like vibrations of substituted benzenes.[56] The region near the anticipated S_0-S_2 origin of HNBPA (ascribable to phenyl ring excitation) is shown in expanded form to the right of the overview spectrum. The hole-burning spectrum of conformer B shows a single, sharp transition at 37 478 cm^{-1}. This transition is −103 cm^{-1} from the S_0-S_1 origin of *N*-benzylacetamide (37 581 cm^{-1}, Figure 3), and lacks the torsional vibrational structure that accompanies the S_0-S_1 transitions of HNBPA(B). Both features suggest an assignment of this band to the S_0-S_2 origin of HNBPA(B) involving electronic excitation of the phenyl ring, rather than as a high-lying vibronic band of the S_1 state. The shift of the S_0-S_2 electronic origin of HNBPA(B) to the red of the S_0-S_1 origin of *N*-benzylacetamide is consistent with the phenol ring weakly stabilizing the phenyl ring in a perpendicular configuration, perhaps via through-bond coupling along the chain. The lack of torsional vibronic structure is consistent with a structure that is not perturbed significantly by $\pi-\pi^*$ excitation on the phenyl ring, as one might expect for the perpendicular inter-ring geometry of structure **III**.

In fact, the presence of this band in the spectrum of HNBPA(B) and the absence of a corresponding transition in HNBPA(A) are pieces of evidence in support of the assignment of conformers A and B to the folded facing (structure **I**) and folded perpendicular (structure **III**) conformations, respectively. Close-up scans of the S_0-S_2 origin (Figure 9b) indicate that the full-width at half-maximum (∼3 cm^{-1}) of the S_0-S_2 origin transition of conformer B is no wider than transitions in the region of the S_0-S_1 origin (where the bandwidth is determined by the rotational band contour, with $\tau(S_1) \approx 10$ ns). Taking the fwhm as an upper limit to the bandwidth puts a lower bound on the $S_2 \rightarrow S_1$ internal conversion lifetime of ∼2 ps for conformer B.

By contrast, the corresponding S_0-S_2 origin of HNBPA(A) is noticeably absent from its UVHB spectrum (Figure 9a). The most likely explanation for this absence is that the folded facing geometry of conformer A is ideally set for excimer-like coupling between the two aromatic rings, leading to fast EET from S_2 to S_1. If this is the case, the S_0-S_2 vibronic transitions would be lifetime broadened by strong coupling to the dense manifold of S_1 vibronic bands, to the point that S_2 vibronic transitions are not observed in the spectrum. It is also possible that strong electronic coupling could lead to large geometry changes that spread the Franck−Condon profile over many vibronic transitions and shift the maximum further to the blue, outside of the wavelength range scanned in the present work.

If the short S_2 lifetime of conformer A is the reason for its apparent absence in the spectrum, this result is consistent with our expectations for the dependence of the rate of electronic energy transfer (EET) on the distance and relative orientations of the donor and acceptor chromophores.[55] As Table 2 summarizes, the folded perpendicular structure **III** assigned to conformer B has a larger inter-ring separation $R_{\pi-\pi}$ (5.1 Å) than in conformer A (4.3 Å, structure **I**). Furthermore, structure **III** also has an interchromophore orientation that is nearly perpendicular (99°, Table 2), which minimizes the interchromophore electronic coupling, while structure **I** is more nearly face-to-face (27°).[55] Given the close proximity of the two chromophores in both structures, the approximations inherent to Forster theory are likely to break down, possibly in spectacular fashion. In this respect, HNBPA could serve as a useful model system for testing theories of electronic energy transfer when the chromophores are in close proximity.[55]

V. Conclusions

In this study, double resonance spectroscopy has been used to record the infrared and ultraviolet spectra of single conforma-

tions of the model flexible bichromophore, HNBPA. The characteristic amide NH and OH stretch frequencies allow for the conformational assignments of the experimentally observed conformers to folded facing (conformer A) and folded perpendicular (conformer B) geometries. The HNBPA molecule is also an ideal test system for electronic structure methods as the various conformers explore a range of separations and orientations between the two aromatic rings, with structures that are extraordinarily sensitive to dispersive interactions. Finally, HNBPA shows evidence for conformation specific electronic energy transfer in which the S_0-S_2 transition in the folded-facing conformer A is not observed, while that in the folded-perpendicular conformer B has a single sharp transition ascribed to the S_0-S_2 origin, with a width consistent with electronic energy transfer on the picosecond or longer time scale.

Acknowledgment. T.S.Z. and E.E.B. gratefully acknowledge support from the National Science Foundation Experimental Physical Chemistry program (CHE 0551075) for this research. T.H.C. and K.D.J. acknowledge support from the National Science Foundation under grant CHE 0518253.

References and Notes

(1) Chin, W.; Compagnon, I.; Dognon, J. P.; Canuel, C.; Piuzzi, F.; Dimicoli, I.; von Helden, G.; Meijer, G.; Mons, M. *J. Am. Chem. Soc.* **2005**, *127*, 1388.

(2) Chin, W.; Dognon, J. P.; Piuzzi, F.; Dimicoli, I.; Mons, M. *Mol. Phys.* **2005**, *103*, 1579.

(3) Chin, W.; Piuzzi, F.; Dimicoli, I.; Mons, M. *PCCP* **2006**, *8*, 1033.

(4) Abo-Riziq, A.; Bushnell, J. E.; Crews, B.; Callahan, M.; Grace, L.; De Vries, M. S. *Chem. Phys. Lett.* **2006**, *431*, 227.

(5) Abo-Riziq, A.; Crews, B. O.; Callahan, M. P.; Grace, L.; de Vries, M. S. *Angew. Chem., Int. Ed.* **2006**, *45*, 5166.

(6) Shubert, V. A.; Baquero, E. E.; Turk, J. A.; Hare, A. A.; Worrel, K.; Lipton, M. A.; Schofield, D. P.; Jordan, K. D.; Zwier, T. S. *J. Chem. Phys.* **2007**, *127*, 234315.

(7) Lee, C. T.; Yang, W. T.; Parr, R. G. *Phys. Rev.* **1988**, *37*, 785.

(8) Vosko, S. H.; Wilk, L.; Nussair, M. *Can. J. Phys.* **1980**, 58.

(9) Stephens, P. J.; Devlin, F. J.; Chablowski, C. J.; Frisch, M. J. *J. Phys. Chem.* **1994**, 1994.

(10) Holroyd, L. F.; van Mourik, T. *Chem. Phys. Lett.* **2007**, *442*, 42.

(11) Shields, A. E.; van Mourik, T. *J. Phys. Chem. A* **2007**, *111*, 13272.

(12) Moller, C.; Plesset, M. S. *Phys. Rev.* **1934**, *46*, 0618.

(13) Boys, S. B.; Bernardi, F. *Mol. Phys.* **1970**, *19*, 553.

(14) van Mourik, T. *Chem. Phys.* **2004**, *304*, 317.

(15) Zhao, Y.; Truhlar, D. G. *J. Chem. Theory Comput.* **2006**, *2*, 1009.

(16) Kolar, M.; Hobza, P. *J. Phys. Chem. A* **2007**, *111*, 5851.

(17) Sinnokrot, M. O.; Sherrill, C. D. *J. Phys. Chem. A* **2004**, *108*, 10200.

(18) Hobza, P.; Sponer, J. *J. Am. Chem. Soc.* **2002**, *124*, 11802.

(19) Hill, J. G.; Platts, J. A.; Werner, H. *PCCP* **2006**, *8*, 4072.

(20) Sinnokrot, M. O.; Sherrill, C. D. *J. Chem. Phys.* **2006**, *110*, 106.

(21) Janowski, T.; Pulay, P. *Chem. Phys. Lett.* **2007**, *447*, 27.

(22) Lee, E. C.; Kim, D.; Jurecky, P.; Tarekeshwar, P.; Hobza, P.; Kim, K. S. *J. Phys. Chem. A* **2007**, *111*, 3466.

(23) Zhao, Y.; Schultz, N. E.; Truhlar, D. G. *J. Chem. Theory Comput.* **2006**, *2*, 364.

(24) Zhao, Y.; Truhlar, D. G. *J. Chem. Theory Comput.* **2007**, *3*, 289.

(25) Ebata, T.; Suzuki, Y.; Mikami, N.; Miyashi, T.; Ito, M. *Chem. Phys. Lett.* **1984**, *110*, 597.

(26) Zehnacker, A.; Lahmani, F.; Breheret, E.; Desvergne, J. P.; BouasLaurent, H.; Germain, A.; Brenner, V.; Millie, P. *Chem. Phys.* **1996**, *208*, 243.

(27) Zehnacker, A.; Lahmani, F.; Desvergne, J. P.; Bouas-Laurent, H. *Chem. Phys. Lett.* **1998**, *293*, 357.

(28) Latt, S. A.; Cheung, H. T.; Blout, E. R. *J. Am. Chem. Soc.* **1965**, *87*, 995.

(29) Chattoraj, M.; Bal, B.; Closs, G. L.; Levy, D. H. *J. Phys. Chem.* **1991**, *95*, 9666.

(30) Chattoraj, M.; Chung, D. D.; Paulson, B.; Closs, G. L.; Levy, D. H. *J. Phys. Chem.* **1994**, *98*, 3361.

(31) Chattoraj, M.; Paulson, B.; Shi, Y.; Closs, G. L.; Levy, D. H. *J. Phys. Chem.* **1993**, *97*, 13046.

(32) Vandantzig, N. A.; Levy, D. H.; Vigo, C.; Piotrowiak, P. *J. Chem. Phys.* **1995**, *103*, 4894.

(33) Weiner, P.; Kollman, P. *J. Comput. Chem.* **1981**, *2*, 287.

(34) Halgren, T. A. *J. Comput. Chem.* **1996**, *17*, 490.

(35) Mohamadi, F.; Richards, N. G. J.; Guida, W. C.; Liskamp, R.; Lipton, M.; Caufield, C.; Chang, G.; Hendrickson, T.; Still, W. C. *J. Comput. Chem.* **1990**, *11*, 440.

(36) Becke, A. D. *J. Chem. Phys.* **1993**, *98*, 5648.

(37) Frisch, M. J.; Pople, J. A.; Binkley, J. S. *J. Chem. Phys.* **1984**, *80*, 3265.

(38) Frisch, M. J.; Trucks, G. W.; Schlegel, H. B.; Scuseria, G. E.; Robb, M. A.; Cheeseman, J. R.; Montgomery, J. A.; Jr., Vreven, T.; Kudin, K. N.; Burant, J. C.; Millam, J. M.; Iyengar, S. S.; Tomasi, J.; Barone, V.; Mennucci, B.; Cossi, M.; Scalmani, G.; Rega, N.; Petersson, G. A.; Nakatsuji, H.; Hada, M.; Ehara, M.; Toyota, K.; Fukuda, R.; Hasegawa, J.; Ishida, M.; Nakajima, T.; Honda, Y.; Kitao, O.; Nakai, H.; Klene, M.; Li, X.; Knox, J. E.; Hratchian, H. P.; Cross, J. B.; Bakken, V.; Adamo, C.; Jaramillo, J.; Gomperts, R.; Stratmann, R. E.; Yazyev, O.; Austin, A. J.; Cammi, R.; Pomelli, C.; Ochterski, J. W.; Ayala, P. Y.; Morokuma, K.; Voth, G. A.; Salvador, P.; Dannenberg, J. J.; Zakrzewski, V. G.; Dapprich, S.; Daniels, A. D.; Strain, M. C.; Farkas, O.; Malick, D. K.; Rabuck, A. D.; Raghavachari, K.; Foresman, J. B.; Ortiz, J. V.; Cui, Q.; Baboul, A. G.; Clifford, S.; Cioslowski, J.; Stefanov, B. B.; Liu, G.; Liashenko, A.; Piskorz, P.; Komaromi, I.; Martin, R. L.; Fox, D. J.; Keith, T.; Al-Laham, M. A.; Peng, C. Y.; Nanayakkara, A.; Challacombe, M.; Gill, P. M. W.; Johnson, B.; Chen, W.; Wong, M. W.; Gonzalez, C.; Pople, J. A. *Gaussian 03.*, Revision C.02; Gaussian, Inc.: Wallingford, CT, 2004.

(39) Woon, D. E.; Dunning, T. H. *J. Chem. Phys.* **1995**, *103*, 4572.

(40) Dunning, T. H. *J. Chem. Phys.* **1989**, *90*, 1007.

(41) Kendall, R. A.; Dunning, T. H.; Harrison, R. J. *J. Chem. Phys.* **1992**, *96*, 6796.

(42) Grimme, S. *J. Chem. Phys.* **2003**, *118*, 9095.

(43) Saebo, S.; Pulay, P. *J. Chem. Phys.* **2001**, *115*, 3957.

(44) Werner, H. J.; Knowles, P. J.; Lindh, R.; Manby, F. R.; Schutz, M.; Celani, P.; Korona, T.; Rauhut, G.; Amos, R. D.; Bernhardsson, A.; Berning, A.; Cooper, D. L.; Deegan, M. J. O.; Dobbyn, A. J.; Eckert, F.; Hampel, C.; Hetzer, G.; Lloyd, A. W.; McNicholas, S. J.; Meyer, W.; Mura, M. E.; Nicklass, A.; Palmieri, P.; Pitzer, R.; Schumann, U.; Stoll, H.; Stone, A. J.; Tarroni, R.; Thorsteinsson, T. *MOLPRO*, a package of ab initio programs version 2006.1, http://www.molpro.net.

(45) Hampel, C.; Petersson, K. A.; Werner, H. *Chem. Phys. Lett.* **1992**, *190*, 1.

(46) Florio, G. M.; Christie, R. A.; Jordan, K. D.; Zwier, T. S. *J. Am. Chem. Soc.* **2002**, *124*, 10236.

(47) Chin, W.; Dognon, J. P.; Canuel, C.; Piuzzi, F.; Dimicoli, I.; Mons, M.; Compagnon, I.; von Helden, G.; Meijer, G. *J. Chem. Phys.* **2005**, 122.

(48) Chin, W.; Mons, M.; Dognon, J. P.; Mirasol, R.; Chass, G.; Dimicoli, I.; Piuzzi, F.; Butz, P.; Tardivel, B.; Compagnon, I.; von Helden, G.; Meijer, G. *J. Phys. Chem. A* **2005**, *109*, 5281.

(49) Abo-Riziq, A. G.; Bushnell, J. E.; Crews, B.; Callahan, M. P.; Grace, L.; De Vries, M. S. *Int. J. Quantum Chem.* **2005**, *105*, 437.

(50) Yamada, Y.; Mikami, N.; Ebata, T. *J. Chem. Phys.* **2004**, *121*, 11530.

(51) Davidsson, J.; Gutow, J. H.; Zare, R. N. *J. Phys. Chem.* **1990**, *94*, 4069.

(52) Fujimaki, E.; Fujii, A.; Ebata, T.; Mikami, N. *J. Chem. Phys.* **1999**, *110*, 4238.

(53) Ishiuchi, S.; Fujii, M.; Robinson, T. W.; Miller, B. J.; Kjaergaard, H. G. *J. Phys. Chem. A* **2006**, *110*, 7345.

(54) *Advances in Chemical Physics*; Wales, D. J.; Doye, P. K.; Miller, M. A.; Mortenson, P. N.; Walsh, T. R., Eds.; Wiley: New York, 2000; Vol. 115, pp 1.

(55) Scholes, G. D. *Annu. Rev. Phys. Chem.* **2003**, *54*, 57.

(56) Wilson, E. B. *Phys. Rev.* **1934**, *45*, 0706.

JP806787P